



Selective transformation of glycerol into 1,2-propanediol on several Pt/ZnO solids: Further insight into the role and origin of catalyst acidity

V. Montes^a, M. Boutonnet^b, S. Järås^b, A. Marinas^{a,*}, J.M. Marinas^a, F.J. Urbano^a

^a Organic Chemistry Department, University of Córdoba, Campus de Excelencia Internacional Agroalimentario, ceiA3, Marie Curie Building, E-14014 Córdoba, Spain

^b KTH (Royal Institute of Technology), Chemical Technology, Teknikringen 42, SE-100 44 Stockholm, Sweden

ARTICLE INFO

Article history:

Received 9 May 2014

Received in revised form

11 September 2014

Accepted 3 November 2014

Available online xxxx

Keywords:

Glycerol transformation

Microemulsion technique

Pt/ZnO

1,2-Propanediol

Role of acid sites

Effect of chlorine

ABSTRACT

Microemulsion technique allowed us to synthesize different ZnO solids with similar particle sizes and textural properties. Platinum was subsequently incorporated by deposition–precipitation and impregnation methods and solids tested for glycerol selective transformation into 1,2-PDO. Incorporation of platinum led to the creation of new (mainly Lewis) acid sites. A good correlation between conversion and acidity of Pt/ZnO solids was obtained. Interestingly, despite exhibiting some acidity, supports alone were inactive in the process which evidenced the role of the metal in dehydration of glycerol into acetol. Furthermore, as the reaction proceeded some chlorine coming from the precursor (H_2PtCl_6) was leached which led to the disappearance of the strongest acid sites, associated to side reactions (catalytic cracking) thus resulting in an increase in selectivity to 1,2-PDO. Eventual formation of Pt–Zn alloy upon reduction of the systems at ca. 400 °C was beneficial to 1,2-PDO selectivity.

© 2014 Elsevier B.V. All rights reserved.

1. Introduction

Glycerol is a by-product from biodiesel production (ca. 100 kg of glycerol per ton of biodiesel produced). Therefore, its valorization through transformation into other valuable chemicals is of great interest. One of those valuable products is 1,2-propanediol (1,2-PDO), which is used in food industry, as a less toxic alternative to 1,2-ethanediol in antifreeze and as a deicer or as a feedstock in the preparation of polyester resins, just to cite some examples of applications [1]. This chemical is traditionally obtained through the petrochemical route via hydration of propylene oxide. Alternatively, 1,2-PDO could be produced through a biomass route from glycerol via dehydration of primary hydroxyl group (thus forming acetol) followed by hydrogenation of acetol into 1,2-PDO [2].

There are different features affecting activity and selectivity of glycerol transformation on metals, such as the metal of choice (e.g. Pt [3,4], Rh [5,6], Pd [5,7], Ir [8], Cu [9–11]) the addition of a second metal [12,13], of acid or basic additives [5,14], the metal

particle size [15,16] or the support [17,18], just to cite some of them.

As for the mechanistic studies, there are some discrepancies in the literature concerning the nature of active sites responsible for selective transformation of glycerol into 1,2-PDO, in particular for initial dehydration of glycerol into acetol. Selective dehydroxylation of polyols can proceed through 3 different mechanisms. (i) E1 (acid-catalyzed), involving protonation of a hydroxyl group which is then expelled as water, the resulting carbocation being neutralized by the elimination of a neighboring proton; (ii) E2 (base-catalyzed) involving simultaneous H^+ removal, loss of the OH and formation of C=C bond and (iii) homolytic cleavage of a C–O bond on a metallic surface (hydrogenolysis). Therefore, on acidic systems E1 mechanism is followed. In principle, dehydration of glycerol could take place through the primary or the secondary hydroxyl group, the former being thermodynamically favored [19].

According to Zhu et al. [20] Brønsted acid sites catalyze 1,3-propanediol formation whereas Lewis acid sites lead to 1,2-propanediol. On the contrary, Peng et al. [21] speculate on Brønsted acid sites being responsible for glycerol dehydration processes in aqueous medium given the fact that Lewis acid sites would be converted into Brønsted centers. As for the strength needed for the process, in a study on gas phase hydrogenolysis of glycerol

* Corresponding author. Tel.: +34 957218622; fax: +34 957212066.

E-mail address: alberto.marinas@uco.es (A. Marinas).

catalyzed by Cu/ZnO/MOx ($\text{MOx} = \text{Al}_2\text{O}_3$, TiO_2 , and ZrO_2) solids, Feng et al. [22] concluded that strong acid sites were responsible for 1,2-PDO formation whereas weak acid sites led to 1,3-PDO. In the liquid phase, Vasiliadou et al. [18] found that moderate acid sites are sufficient to activate glycerol dehydration. Finally, some studies give support to the role of the metal not only in hydrogenation of acetol but also in glycerol activation [18,23,24].

In a previous paper, a screening of different partially reducible oxides to be used as supports for platinum was described, ZnO being selected for subsequent studies [4]. Moreover, systems reduced at 200 °C exhibited better catalytic performance than those reduced at 400 °C, a temperature at which Pt-Zn alloy was formed which was detrimental to activity. In a follow-up study [24], different solids consisting in a noble metal supported on ZnO were synthesized through the microemulsion method. This allowed us to obtain quite similar metal (Pt, Rh, Pd) particle sizes. Under our experimental conditions, reactivity followed the order Rh > Pt > Pd. Furthermore, the presence of some remaining surfactant seemed to somehow hinder hydrogenation activity of the metal, thus leading to an unusually high selectivity to acetol.

In the present paper, the good control of particle size ensured through microemulsion (ME) technique is used to synthesize diverse ZnO solids (either alone or modified with Al, Ce or Zr) with a view to tune acidity of the support. Platinum is subsequently incorporated onto the systems through deposition–precipitation technique or impregnation from H_2PtCl_6 aqueous solutions. For comparative studies, a system starting from a different precursor (platinum nitrate) was also synthesized. The final goal is to cast further light on the nature and origin of active sites responsible for the initial dehydration step of glycerol into acetol.

2. Experimental

2.1. Materials

Synperonic 13/6.5 was a gift from Croda. Zn(II)-2-ethylhexanoate (89%) dissolved in mineral spirit, Al(III)-2-ethylhexanoate, Zr(IV)-2-ethylhexanoate, Ce(IV)-2-ethylhexanoate, and 15% (w/w) Pt(IV) nitrate solution were purchased from Alfa Aesar. 8 wt% of H_2PtCl_6 aqueous solution, ZnO nanopowder, acetone (technical grade), glycerol 99%, 1,2-propanediol 99.5%, 1,3-propanediol 98%, (hydroxyacetone) acetol 95%, ethylenglycol 99.5%, n-propanol 99.5%, n-hexane > 99%, HCl 33% in water, and NaOH > 99% were purchased from Sigma-Aldrich. Milli-Q water was used for preparation of water solutions.

2.2. Synthesis of the solids

2.2.1. Synthesis of ZnO solids through ME technique

The solids, ZnO (either alone or doped with 5 wt% of Al, Zr or Ce) were synthesized using the commonly known method of oil in water (O/W) microemulsion (ME) [25]. The internal structure of the ME is determined by the relative fractions of three constituents: surfactant, oil and water. The ME is only formed for certain ratios of the constituents, outside which a two-phase system is formed. The first step was to determine the relative fractions of components where the ME was stable. So, different composition mixtures of surfactant and water were prepared at different temperatures. Then a solution of organometallic precursor was added dropwise in order to know the maximum soluble amount. Determination of this amount is easy because the microemulsions are isotropic and transparent, and when they destabilize the transparent dissolution turns into a cloudy system. These experiments allowed us to determine the region of relative fractions of constituents to form microemulsion. Under optimized conditions, the composition of

microemulsions (ME) was surfactant: synperonic 13/6.5 (18.8 wt%), oil: organic precursor of metal (10 wt% of Zn) dissolved in n-hexane (24.5%), water: 56.7 wt%. In the case of doping of ZnO with Al, Ce or Zr, the oil is formed by 10 wt% Zn + (Al, Ce or Zr). Moreover, Al, Ce or Zr content was calculated to have 5 wt% of these metals in the resulting ZnO solid.

Once the microemulsion had been obtained in the presence of the Zn(II) ethylhexanoate aqueous solution, pH was increased up to 11 with NH₄OH in order to precipitate ZnO [26]. Resulting solids were aged under stirring for 7 h, centrifuged and carefully washed with 3 portions of 100 mL n-hexane. The solids were dried at 70 °C for 12 h and calcined at 400 °C for 2 h at a rate of 10 °C/min with a synthetic air flow of 2 L/h.

For comparative purposes, a commercial ZnO solid was also used as the support in the present study.

2.2.2. Incorporation of platinum

2.2.2.1. Deposition precipitation method. The synthetic procedure was as follows: a volume of 6.57 mL of chloroplatinic acid solution (or 1.67 mL of Pt(NO₃)₄ solution) was diluted to 200 mL with Milli-Q water and adjusted to pH 7 by adding 0.1 M NaOH. Then, an amount of 4.75 g of support was added and the mixture readjusted to pH 7 with 0.1 M HCl. The solution containing the support was refluxed at 70 °C under vigorous stirring for 2 h. Then, a volume of 10 mL of isopropanol was added, the temperature raised to 110 °C and refluxing continued for 30 min, after which the mixture was vacuum filtered and the filtrate washed with 3 portions of 25 mL of water each. The resulting solid was dried in a muffle furnace at 110 °C for 12 h, ground and calcined at 400 °C for 4 h with a rate of 1 °C/min. After calcination, the solid was ground again, sieved through a mesh of 0.149 mm pore size and stored in a flask.

2.2.2.2. Impregnation method. 200 mL of water containing the metal precursor (chloroplatinic acid) was adjusted to pH 7 with NaOH. Then, the corresponding amount of ZnO solid (in order to obtain 5 wt% Pt/ZnO in final systems) was suspended and pH readjusted to 7 with HCl. Suspensions were stirred for 5 h at room temperature and then the solvent was rota-evaporated and calcined at 400 °C. After calcination, the solid was ground, sieved through a mesh of 0.149 mm pore size and stored in a flask.

The nomenclature of the solids includes an N or Cl prefix indicating the platinum precursor (platinum nitrate or chloroplatinic acid, respectively), followed by the method of incorporation (dp or im for deposition–precipitation or impregnation, respectively) and the origin of the ZnO used (com or ME for commercial or synthesized through microemulsion, respectively). In the latter case, when applicable, Al, Ce or Zr refers to the metal doping ZnO. Finally, the name is followed by the reduction treatment. Therefore, for instance, a catalyst synthesized by deposition–precipitation method from chloroplatinic acid on an Al-doped ZnO solid synthesized through microemulsion and pre-reduced at 200 °C is denoted as Cl-dp-ME-Al-200 whereas N-dp-com-unred would indicate that platinum nitrate was incorporated on a commercial ZnO through deposition–precipitation method and tested in the reaction without any reduction pre-treatment.

2.3. Characterization

Elemental analysis of metal-containing samples was performed by the staff at the Central Service for Research Support (SCAI) of the University of Córdoba. It was performed using inductively coupled plasma mass spectrometry (ICP-MS). Measurements were made on a Perkin-Elmer ELAN DRC-e instrument following dissolution of the sample in a 1:3 HNO₃/HCl mixture with a soft heating. Calibration was done by using PE Pure Plus atomic spectroscopy standards, also from Perkin-Elmer.

Thermogravimetric analyses (TGA–DTA) were performed on a Setaram SetSys 12 instrument. An amount of 20 mg of sample was placed in an alumina crucible and heated at temperatures from 30 to 1000 °C at a rate of 10 °C/min under a stream of synthetic air at 40 mL/min in order to measure weight loss, heat flow and derivative weight loss.

EDX measurements were performed on a JEOL JSM-6300 scanning electron microscope (SEM) equipped with an energy-dispersive X-ray (EDX) detector. It was operated at an acceleration voltage of 20 keV with a resolution of 65 eV.

Surface areas of the solids were determined from nitrogen adsorption–desorption isotherms obtained at liquid nitrogen temperature on a Micromeritics ASAP-2010 instrument, using the Brunnauer–Emmett–Teller (BET) method. All samples were degassed to 0.1 Pa at 120 °C prior to measurement.

Transmission electron microscopy (TEM) images were obtained using a JEOL JEM 1400 microscope. All samples were mounted on 3 mm holey carbon copper grids. Particle sizes were obtained by counting 100 particles.

X-ray patterns of the samples were obtained on a Siemens D-5000 diffractometer equipped with a DACO-MP automatic control and data acquisition system. The instrument was equipped with a graphite monochromator and used Cu K α radiation. Metal particle sizes were calculated using Scherrer equation.

X-ray photoelectron spectroscopy (XPS) data were recorded on 4 mm × 4 mm pellets 0.5 mm thick that were obtained by gently pressing the powdered materials following outgassing to a pressure below about 2×10^{-8} Torr at 150 °C in the instrument pre-chamber to remove chemisorbed volatile species. The main chamber of the Leibold–Heraeus LHS10 spectrometer used, capable of operating down to less than 2×10^{-9} Torr, was equipped with an EA-200MCD hemispherical electron analyser with a dual X-ray source using AlK α ($h\nu = 1486.6$ eV) at 120 W, at 30 mA, with C (1s) as energy reference (284.6 eV).

Temperature-programmed reduction (TPR) measurements were made with a Micromeritics TPD-TPR 2920 analyser. An amount of 100 mg of catalyst was placed in the sample holder and reduced in a 10:90 H₂/Ar stream flowing at 20 mL/min. The temperature was ramped from 50 to 350 °C.

Surface acidity in the catalysts were determined by thermal programmed desorption (TPD) of a pre-adsorbed probe molecule, pyridine (Py) monitored by TCD. An amount of 50 mg of sample was placed under a He stream flowing at 75 mL/min in a reactor 10 mm in diameter that was placed inside an oven. The He stream was used to clean the solids by heating to 350 °C at a rate of 10 °C/min and then cooling to 50 °C. At that point, the surface of the solid was saturated with the Py for 30 min. Pyridine was supplied by bubbling the He stream through liquid pyridine at room temperature over the samples. After saturation, excess physisorbed Py was removed increasing the temperature up to 50 °C and passing a He stream at 75 mL/min for 60 min. Then temperature was increased up to 400 °C at 10 °C/min, holding the final level for 30 min. Desorbed pyridine was quantified against a calibration graph previously constructed from variable injected volumes of pyridine.

The above-described overall acidity study by TPD-Py was supplemented with one by diffuse reflectance infrared (DRIFT) spectroscopy of the pyridine-saturated solids intended to identify the specific types of acid sites present. Measurements were made with an ABB Bomen MB Series IR spectrophotometer equipped with a SpectraTech P/N 0030-100 environmental chamber including a diffuse reflectance device capable of performing 258 scans at 8 cm⁻¹ resolution at an adjustable temperature. Prior to analysis, each catalyst was thermally cleaned at 400 °C for 30 min. The last few minutes of the thermal treatment were used to record reference spectra.

2.4. Catalytic tests

Hydrogenolysis of glycerol was conducted in a Berghof HR-100 stainless steel high-pressure autoclave equipped with a 75 mL PTFE vessel and a magnetic stirrer. Under standard conditions, 10 mL of a 1.36 M solution of glycerol in water and 100 mg catalysts were introduced in the vessel. Reactor was then purged with the selected atmosphere (H₂ or N₂), and temperature (180 °C) and pressure (2 or 6 bar) adjusted. The stirring rate was 1200 rpm. After 15 h of reaction, stirring was stopped and the vessel cooled with an ice bath. The reaction mixture was centrifuged to separate the catalyst and the liquid passed through a filter of PTFE 0.45 μm. Then it was analyzed by GC-FID (Agilent Technologies 7890, with a Supelco 25357 NukolTM capillary column). Quantification was carried out through the corresponding calibration curves.

3. Results and discussion

3.1. Characterization of support

TG-DTA profiles of all uncalcined solids obtained through ME method are quite similar. Fig. 1 shows that of ME system. There are two main weight losses centered at ca. 140 °C and 330 °C, respectively. The first one could be due to water whereas the second one could be attributed to the decomposition of remaining organic compounds (e.g. surfactant, organic precursor) [27,28]. In fact, the loss weight % (41.6%) is much higher than the theoretical one corresponding to the conversion of Zn(OH)₂ into ZnO (ca. 18.1%) thus evidencing the presence of remaining organics. Interestingly, there is no significant weight loss at temperatures above calcination temperature (400 °C). In fact, TG-DTA profile of the solid calcined at 400 °C (Fig. 1) did not exhibit any weight loss thus ensuring thermal stability of the obtained solid.

The main features concerning characterization of the supports are given in Table 1. As can be seen, and as expected, ME method ensured quite similar particle sizes (22–26 nm) for all ZnO-based solids, BET surface areas being in the 27–36 m²/g range. For comparative purposes, commercial ZnO solid has also being included in Table 1, its surface area being significantly lower (15 m²/g). In all

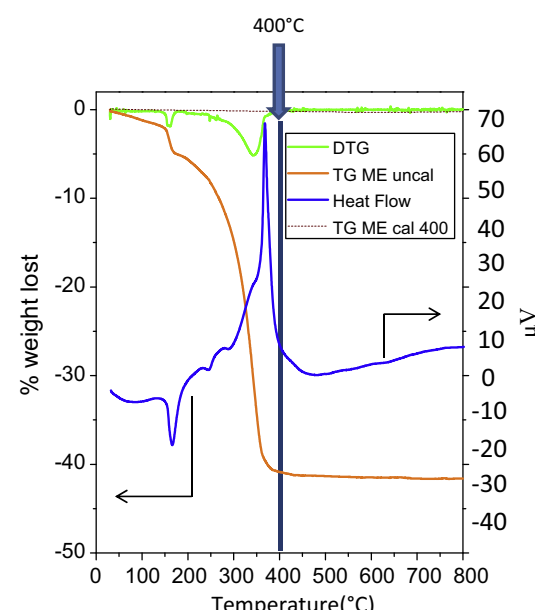


Fig. 1. TG-DTA profile obtained in synthetic air for the ME uncalcined system. Dotted line corresponds to weight loss of ME calcined at 400 °C.

Table 1

Some features concerning characterization of ZnO supports.

Support	N ₂ isotherms		Particle size diameter (XRD)	Metal content (%)			Acidity (μmol py per mg catalyst)
	BET area (m ² /g)	Mean pore diameter (nm)		ICP-MS	EDX	XPS	
Com	15	11	50	–	–	–	0.05
ME	29	8	26	–	–	–	0.08
ME-Al	27	9	23	0.36	0.46	1.65	0.15
ME-Ce	31	7	22	0.53	3.67	3.44	0.15
ME-Zr	36	8	24	0.19	1.26	1.61	0.12

cases, ZnO-systems are mesoporous solids, with mean pore diameters ranging 7–11 nm. As regards elemental analyses of samples, bulk analyses (ICP-MS and EDX) reveal that the metals (Al, Ce or Zr) have been incorporated below the nominal value (5 wt%). One possible reason could be the partial re-dissolution of precipitated hydroxides at the high pH (11) used in the synthesis [29,30]. X-ray diffractograms of ZnO supports (not shown) revealed that in all cases ZnO have a zincite (wurzite) structure with the typical peaks at 2θ values of 31.7, 34.4, 36.2° corresponding to (1 0 0), (0 0 2) and (1 0 1) reflections, respectively [31]. No signals corresponding to ceria, zirconia or alumina were observed which is hardly surprising considering the above-mentioned low incorporation. Acidity of the solids was determined by TPD of pre-adsorbed pyridine (Table 1). Interestingly, despite the relatively low metal-doping content, incorporation of Al, Ce or Zr led to a significant increase in acidity, in the 50–88% range. Moreover, acidity of commercial ZnO solid is lower than that of the pure ZnO system obtained through microemulsion technique. No change in acidity of the supports was observed after treatment under H₂ flow for 2 h at 200 °C or 400 °C.

3.2. Characterization of platinum-containing solids

Some features concerning characterization of Pt-containing systems are summarized in Table 2. ICP-MS results confirm a good incorporation of platinum, quite close to the nominal content (5 wt%).

XRD profiles of the samples (Fig. 2) reveal that in general, reduction at 200 °C results in the appearance of a band at ca. 39.8° attributed to (1 1 1) crystal plane of the Pt⁰ face-centered-cubic phase [32] whereas subsequent reduction at 400 °C leads to the shift of the band to higher 2θ values (ca. 40.9°) which is indicative of the formation of Pt-Zn alloy [4,33]. The exceptions are Cl-dp-ME-Ce and Cl-im-com systems. In the former case, unred system already exhibits a signal at ca. 39.8° which could be indicative of some kind of Pt-support interaction (Pt-Zn or Pt-Ce [34]). In the latter case, Pt-Zn alloy seems to be already present in the solid reduced at 200 °C (see signal at ca. 45.9°). In any case, the influence of other factors on the appearance of Pt bands (e.g. metal particle size, oxidation state) should be studied by other techniques (e.g. TEM, XPS).

H₂ TPR profiles are shown in Fig. 3. There are different factors affecting reducibility of metal particles such as size, the metal

environment (e.g. presence of chloride species coming from the precursor) or when using partially reducible oxides as the support, as it is the case of the present study, existence of strong metal–support interactions [35–37]. Therefore, smaller metal particles are more difficult to be reduced than larger ones thus resulting in a shift to higher temperatures in the TPR profile. Moreover, the presence of chloride ions at the metal–support interface has been described to hinder electron exchange between the metal and the oxide support thus leading to higher reduction temperatures. Finally, reduction peaks appearing at the highest reduction temperatures are typically associated to those platinum particles strongly interacting with the support. Fig. 3 confirms that at the temperature selected for catalytic experiments (180 °C) all systems are reduced. Furthermore, TPR signals of all the systems obtained through ME exhibit a single relatively narrow peak which suggests a homogeneous platinum particle size distribution. As regards the solids based on commercial ZnO, results suggest the influence of both the synthetic method and the metal precursor on metal dispersion. Therefore, a more homogeneous distribution of platinum particle sizes would be expected for Cl-dp-com than for Cl-im-com judging by the narrower TPR peak in the former case. Comparing the effect of the employed Pt precursors (Cl-dp-com vs N-dp-com), larger and more heterogeneous in size platinum particles seem to have been obtained from platinum nitrate, as suggested by the wider TPR profile appearing at lower reduction temperatures. The influence of chlorine residues shifting TPR peaks to higher temperatures in the case of Cl-dp-com, cannot be ruled out. TEM micrographs (Figs. 4–6) cast further light on these issues. The first conclusion that can be drawn from this study is that the average particle sizes for the samples reduced at 200 °C are quite similar for all types of solids (in the 1.3–2.0 nm range, Table 2), the exception being N-dp-com for which larger metal particles (2.8 nm, Fig. 6) were obtained. This could be ascribed to the different metal precursor used and is in line with TPR profiles which evidenced an easier reduction of platinum particles in that solid. If TEM figures of Cl-im-com-200 and Cl-dp-com-200 are compared (Fig. 5), quite similar particle size distributions are obtained. This suggests that above-commented observed differences in TPR and XRD profiles could be ascribed to different metal–support interactions. Finally, in all cases, increase in reduction temperature from 200 °C up to 400 °C resulted in metal sintering.

Table 2

Some features concerning characterization of the different Pt/ZnO solids.

Catalyst	Pt (wt%)		Average Pt particle size (TEM, nm)		Total acidity (μmol py/mg catalyst)			
	ICP-MS	EDX	200	400	Unred	200	400	Used
Cl-dp-com	4.2	2.7	1.9	3.6	0.23	0.14	0.14	0.11
Cl-dp-ME	4.7	3.0	1.8	3.0	0.29	0.20	0.14	0.15
Cl-dp-ME-Al	4.5	3.9	1.7	3.3	0.35	0.21	0.17	0.13
Cl-dp-ME-Ce	6.1	4.0	1.3	2.2	0.30	0.16	0.15	0.11
Cl-dp-ME-Zr	4.8	5.5	1.5	3.2	0.47	0.31	0.16	0.12
Cl-im-com	4.5	2.9	2.0	3.3	0.20	0.11	0.08	0.0
N-dp-com	4.3	6.0	2.8	4.2	0.07	0.06	0.07	0.0

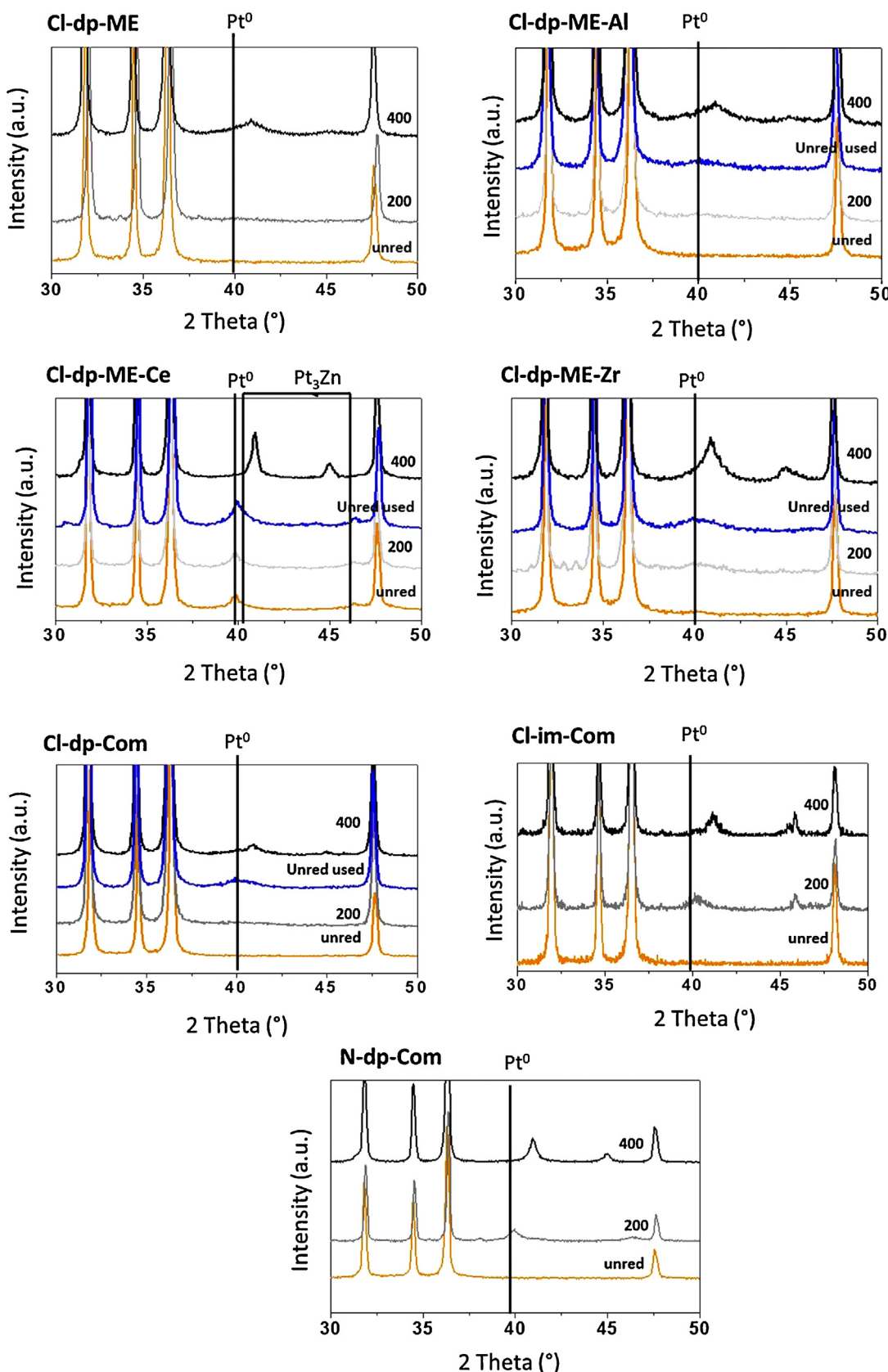


Fig. 2. X-ray diffractograms of the different Pt/ZnO systems unreduced or reduced at 200 °C and 400 °C. In some cases the profiles of unreduced systems after 15 h of reaction have also been included.

XPS spectra of unreduced samples in the Zn 2p_{3/2} region showed a peak centered at ca. 1022 eV which can be ascribed to ZnO. In the case of solids obtained from H₂PtCl₆, reduction at 200 °C resulted in the appearance of a second peak at ca. 1023 eV whose relative intensity decreased upon subsequent reduction at 400 °C (see Fig. 7). This second peak can be associated to oxychlorinated Zn²⁺ species [38]. As regards Pt 4f_{5/2}, unreduced systems are formed by Pt²⁺ (72.4–72.8 eV) and Pt⁴⁺ (73.7–74.9 eV) whereas no signals corresponding to Pt⁰ at ca. 70.6–71.0 eV were observed. Interestingly, the highest Pt²⁺ percentage (ca. 44%) corresponded to Cl-dp-ME-Ce solid which could be ascribed to Ce interacting with Pt (remember XRD profiles, Fig. 2). Reduction of the solids at 200 °C resulted in the formation of Pt⁰ which is concordant with XRD and TPR profiles. As regards XPS spectra of metal-doping species (Fig. 8), Al 2s signals of Cl-dp-ME-Al unreduced and reduced at 200 and 400 °C remained at 118.5 eV which suggests an Al₂O₃ environment [39]. Similarly, Zr 3d_{5/2} signal of Cl-dp-ME-Zr-unred, 200 and 400 °C solids appeared at 182 eV which suggests the presence of ZrO₂ [40]. In contrast, Ce 3d_{5/2} signal of Cl-dp-ME-Ce-unred solid differed from those of the solid reduced at 200 °C and 400 °C thus suggesting different Ce(III)/Ce(IV) ratios in those samples depending on the reduction treatment [34].

TPD profiles of pre-adsorbed pyridine are depicted in Fig. 9 and acidity data are summarized in Table 2. From Fig. 9 it is evident that the incorporation of platinum using H₂PtCl₆ as the precursor led to the creation of acidity. Therefore, there are two main pyridine

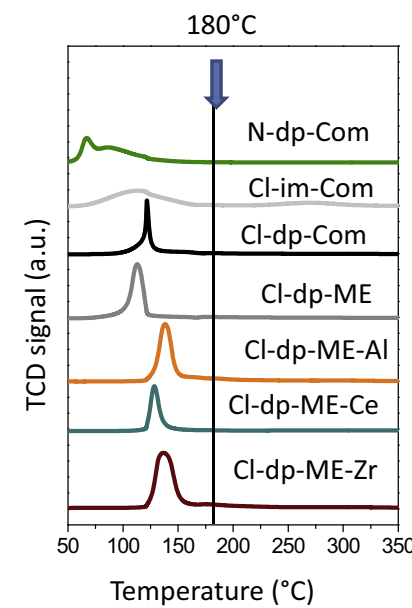


Fig. 3. TPR profiles of the different Pt/ZnO systems. The vertical line indicates reaction temperature in catalytic experiments of glycerol transformation (180 °C).

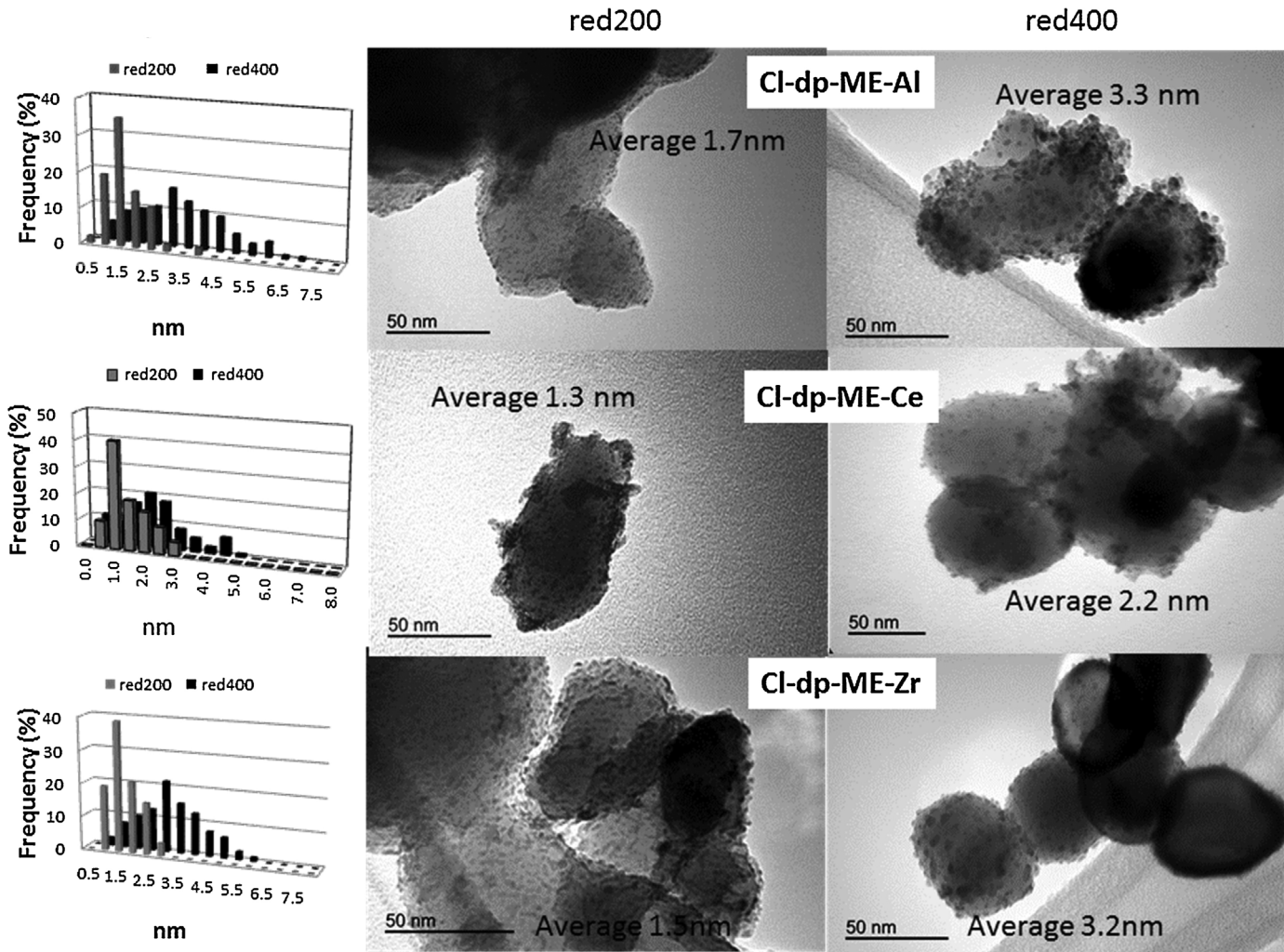


Fig. 4. TEM micrographs of Cl-dp-ME-Al, Cl-dp-ME-Ce and Cl-dp-ME-Zr reduced at 200 and 400 °C.

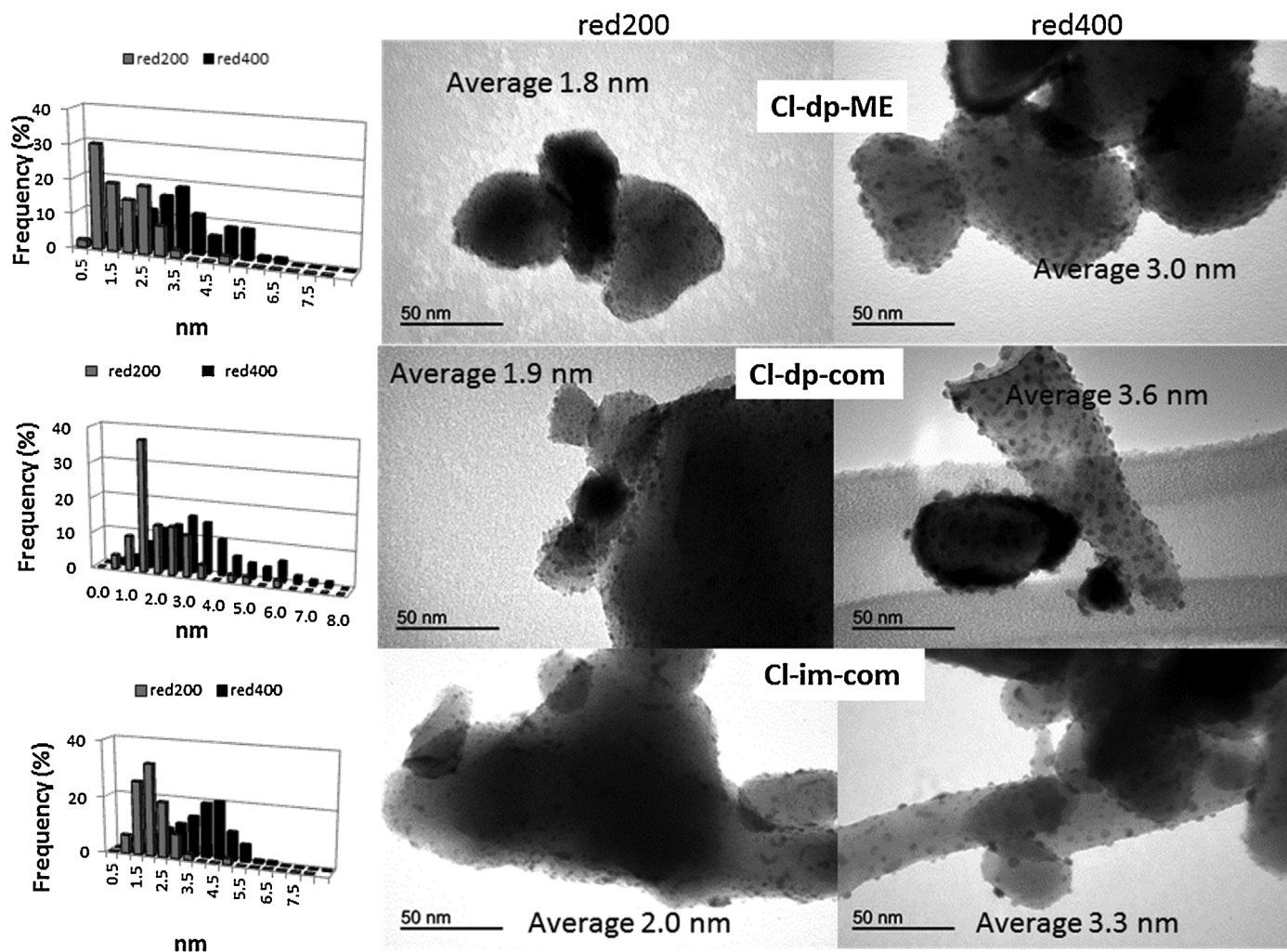


Fig. 5. TEM micrographs of Cl-dp-ME, Cl-dp-com and Cl-im-com reduced at 200 and 400 °C.

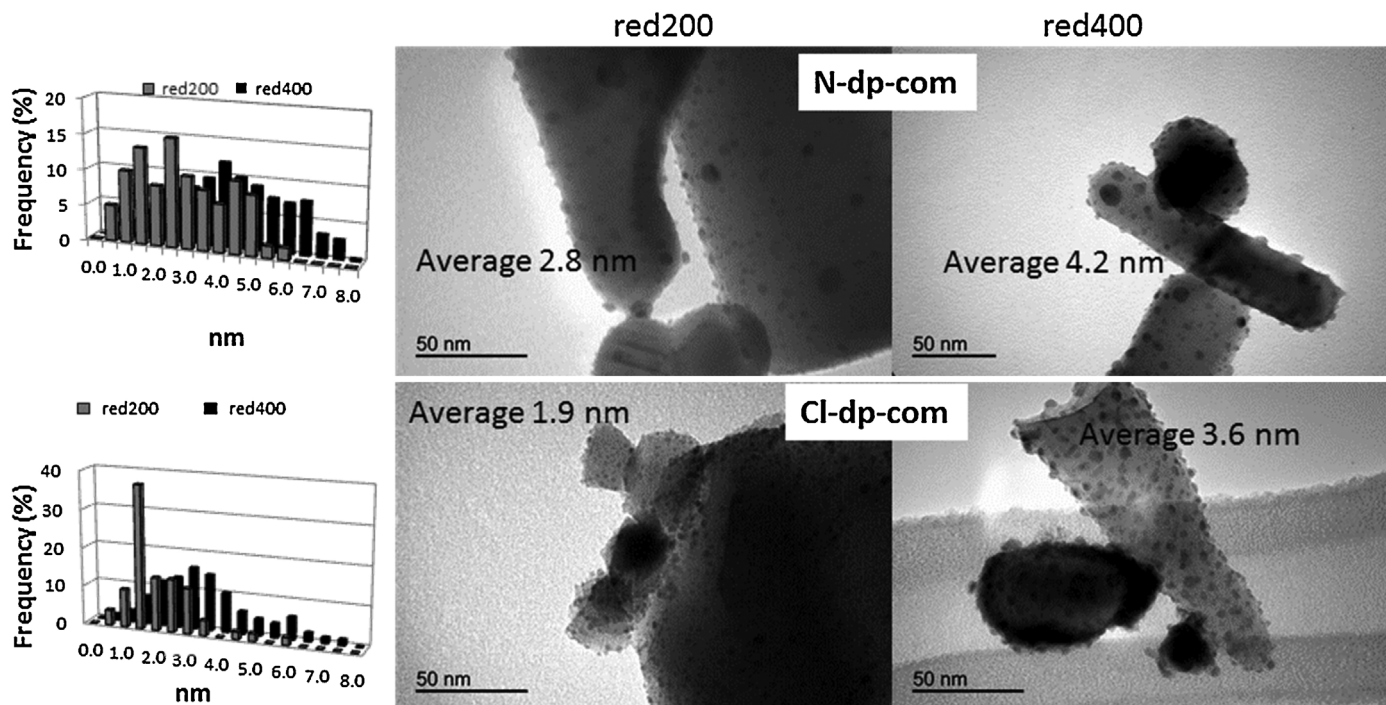


Fig. 6. TEM micrographs of N-dp-com and Cl-dp-com reduced at 200 and 400 °C.

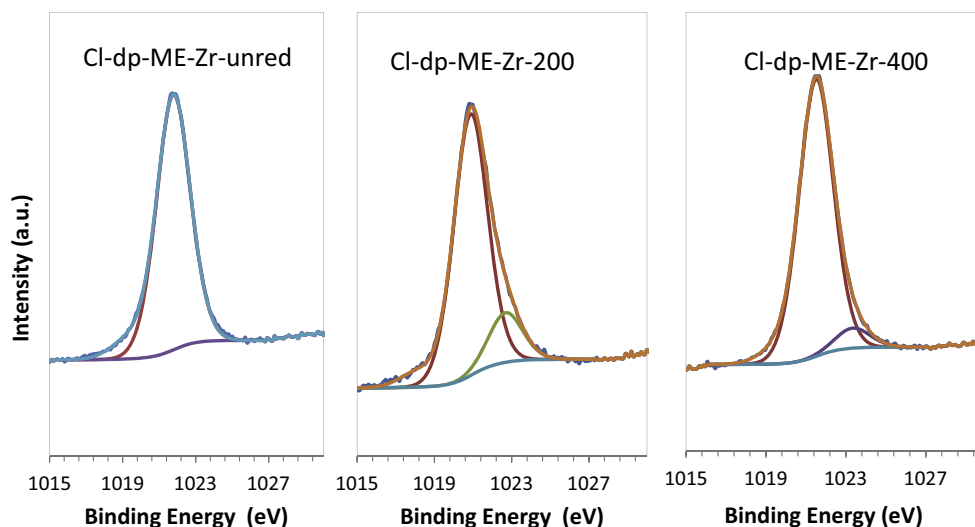


Fig. 7. XPS profiles in the Zn (2p_{3/2}) region of Cl-dp-ME-Zr system unreduced and reduced at 200 °C or 400 °C.

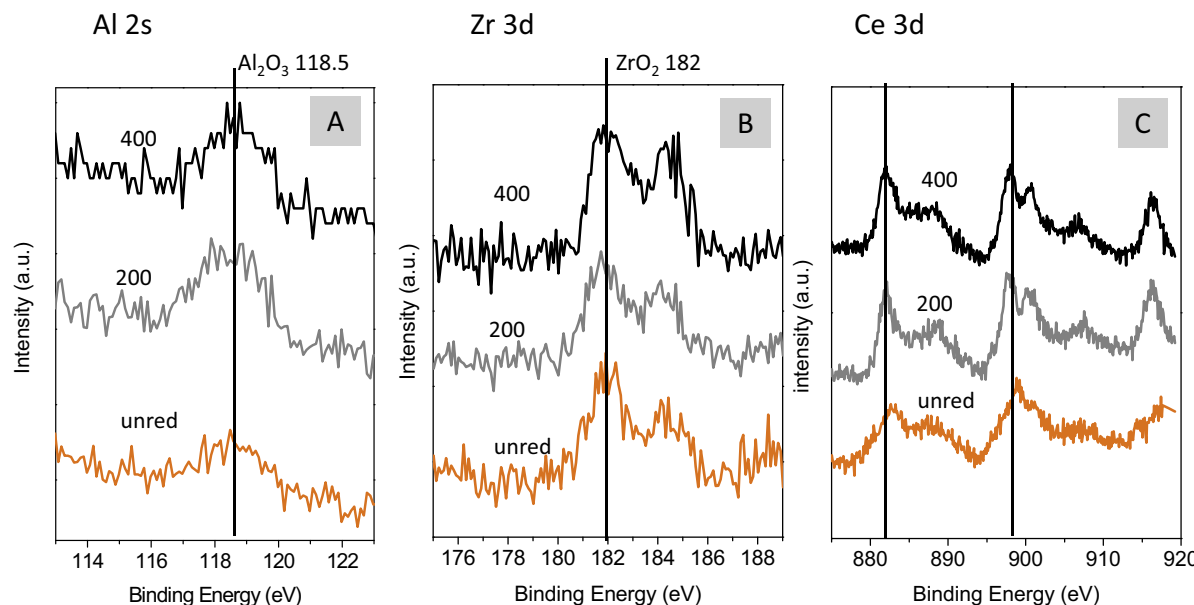


Fig. 8. XPS profiles of Cl-dp-ME-Al (A), Cl-dp-ME-Zr (B) and Cl-dp-ME-Ce (C) unreduced and reduced at 200 °C and 400 °C in the XPS Al (2s), Zr (3d) and Ce (3d) regions, respectively.

desorption peaks centered at ca. 100 °C and 300 °C, respectively. Reduction of the solids at 200 °C results in the disappearance of the high-temperature peak whereas the low-temperature one remains even after reduction at 400 °C. In the case of N-dp-com solid, on the contrary, incorporation of platinum did not result in new acid sites, thus confirming that new acid sites are somehow associated to the presence of chlorine. In order to cast further light on the nature (Lewis or Brønsted) of acid sites, acidity tests were complemented with DRIFT studies. Fig. 10 presents the DRIFT spectra of pyridine chemisorbed on Cl-dp-com solids at different temperatures (100–400 °C) though similar results are obtained for the other systems coming from H₂PtCl₆ precursor. In all cases, the spectra of pyridine adsorbed at 100 °C on unreduced Pt-containing solids exhibit two main bands centered at ca. 1454 and 1610 cm⁻¹ which are associated to Lewis acid sites, together with some other minor ones at ca. 1486 (Brønsted + Lewis), 1547 (Brønsted) [41,42]. Acidity of solids reduced at 200 °C is lower (as evidenced by the decrease in intensity of all bands) whereas subsequent reduction at 400 °C

hardly changes acidity (which is consistent with Fig. 9). Interestingly, N-dp-com-unred solid also exhibited in DRIFT studies the above-mentioned Lewis acid sites which retained pyridine up to 100 °C whereas no bands due to pyridine adsorption were observed for reduced systems (not shown). All these results suggest that on introduction of platinum (either using H₂PtCl₆ or Pt(NO₃)₄ as the precursor) some new acid sites, mainly Lewis-type, are created. In the case of Cl-series some of those sites are kept in reduced solids (probably associated to the presence of chlorine) whereas for N-dp-com reduction at 200 °C leads to their disappearance, which could be due to reduction of Pt(II) and Pt(IV) to Pt⁰ as evidenced by XPS and H₂ TPR studies.

3.3. Catalytic activity

Production of 1,2-PDO from glycerol is known to occur via intermediate production of acetol. Therefore, dehydration of primary hydroxyl group in glycerol yields acetol whose hydrogenation leads

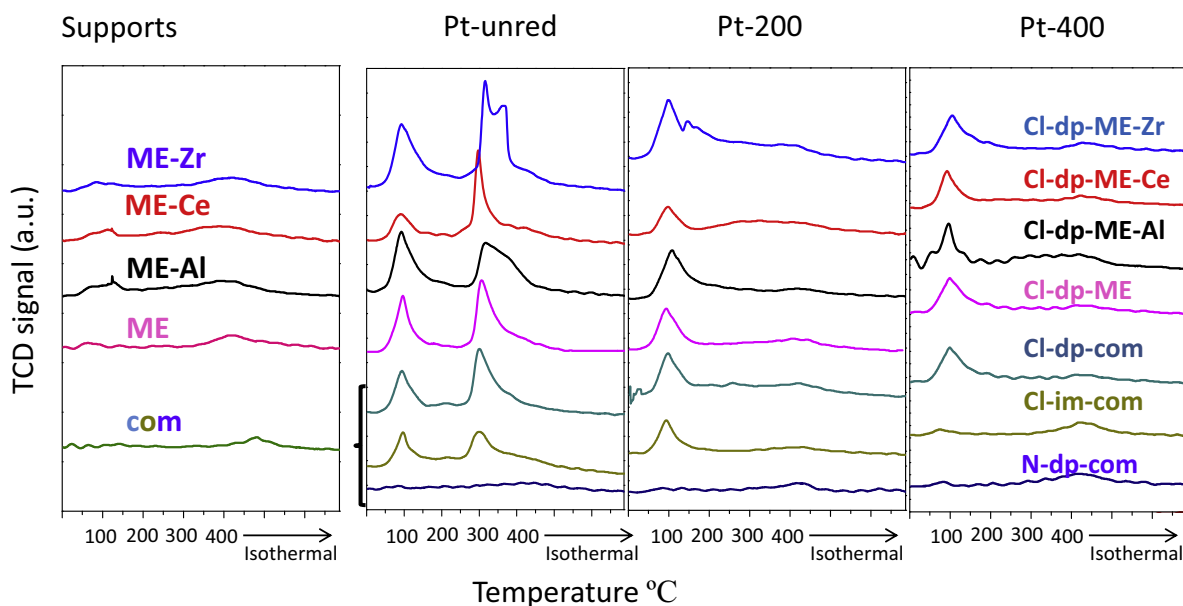


Fig. 9. Temperature-programmed desorption (TPD) profiles of pyridine pre-adsorbed at 50 °C for supports and Pt/ZnO systems (unreduced and reduced at 200 °C and 400 °C).

to 1,2-PDO (**Scheme 1**). The different catalysts were tested for their activity for glycerol transformation into 1,2-PDO. Under standard conditions (see Section 2.4), supports (unreduced or reduced at 200 °C or 400 °C) were not active in the process. As for the Pt-containing solids, results obtained for conversion and selectivity after 15 h reaction are summarized in **Fig. 11**. In terms of conversion, values achieved with unreduced samples are in general quite similar to those obtained for solids reduced at 200 °C. This is hardly surprising since at the working temperature (180 °C) platinum can be *in situ* reduced (remember TPR profiles). Subsequent reduction at 400 °C led to a dramatic decrease in conversion. Increase in

particle size (as evidenced by TEM, **Table 2**) and formation of Pt–Zn alloy (remember XRD results) could account for that. An additional point to take into account is that total acidity decreases with reduction temperature (see **Table 2**) which will be further commented in the mechanistic discussion. It is also worth noting that conversion values for N-dp-com systems are significantly lower than those of their Cl-dp-com counterparts which again could be related to the larger particles. In fact, if TOF values (expressed as moles of glycerol converted per mole of Pt per hour) are represented (**Fig. 12**), N-dp-com and Cl-dp-com perform quite similarly either unreduced and reduced at 200 °C.

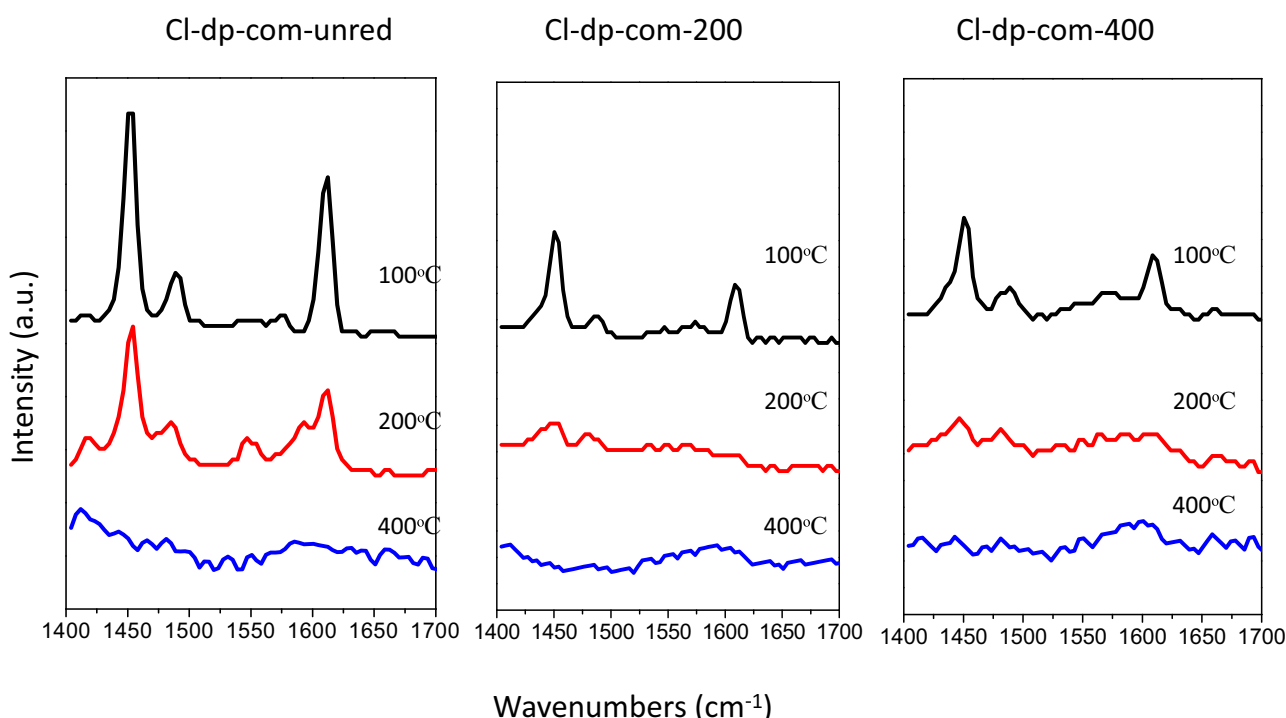
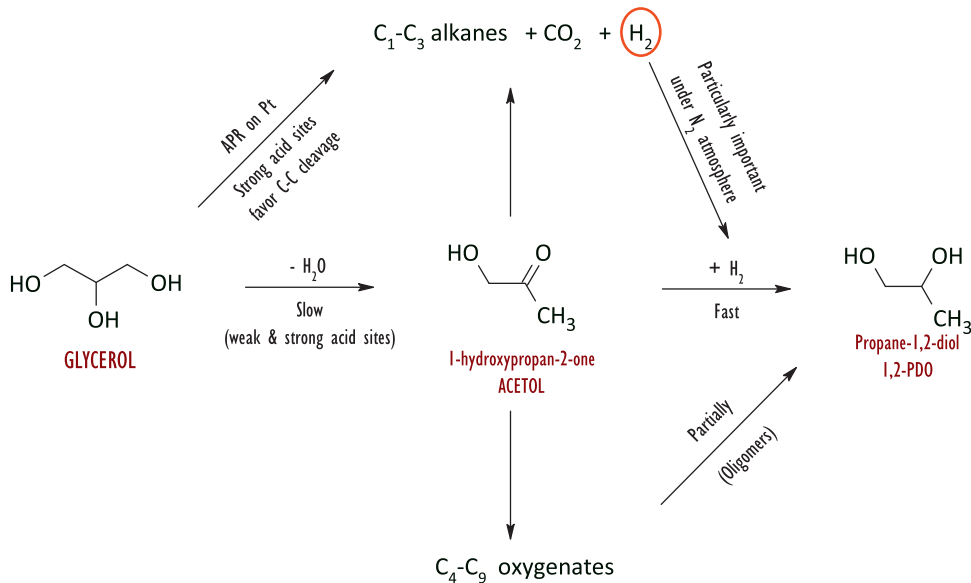


Fig. 10. Diffuse reflectance infrared Fourier transformed spectra (DRIFT) of Cl-dp-com systems saturated with pyridine at 50 °C upon thermal treatment at different temperatures (100, 200 and 400 °C).



Scheme 1. Mechanism proposed for transformation of glycerol under our experimental conditions.

In terms of TOF, Cl-dp-ME-Zr-unred and Cl-dp-Al-unred (the most acidic solids, as determined by TPD of pre-adsorbed pyridine) are the systems exhibiting the highest values whereas Cl-dp-ME-Ce-unred, for which some kind of Pt-support interaction had already been detected by XRD in unred system and Cl-im-com (which apparently also evidenced Pt-support interaction at lower temperatures than its ME counterparts) are the least active solids. Fig. 13 shows a dependence of conversion on acidity and platinum average particle size. From that figure it is evident that the presence of the metal is necessary for the reaction since supports, despite exhibiting some acidity, are inactive in the reaction. This backs

the idea of the metal participating in dehydration of glycerol to acetol.

As far as selectivity to 1,2-PDO is concerned (Fig. 11B), reduction at 400°C resulted in a significant increase up to values of ca. 90%, the exception being N-dp-com and Cl-im-com. However, appropriate study of effect of reduction temperature on selectivity to 1,2-PDO requires the performance of reactions with unred and 200 systems at lower reaction times in order to get similar conversions to those achieved with solids reduced at 400°C after 15 h (i.e. selectivity values must be compared at iso-conversions). This will be performed in the following section.

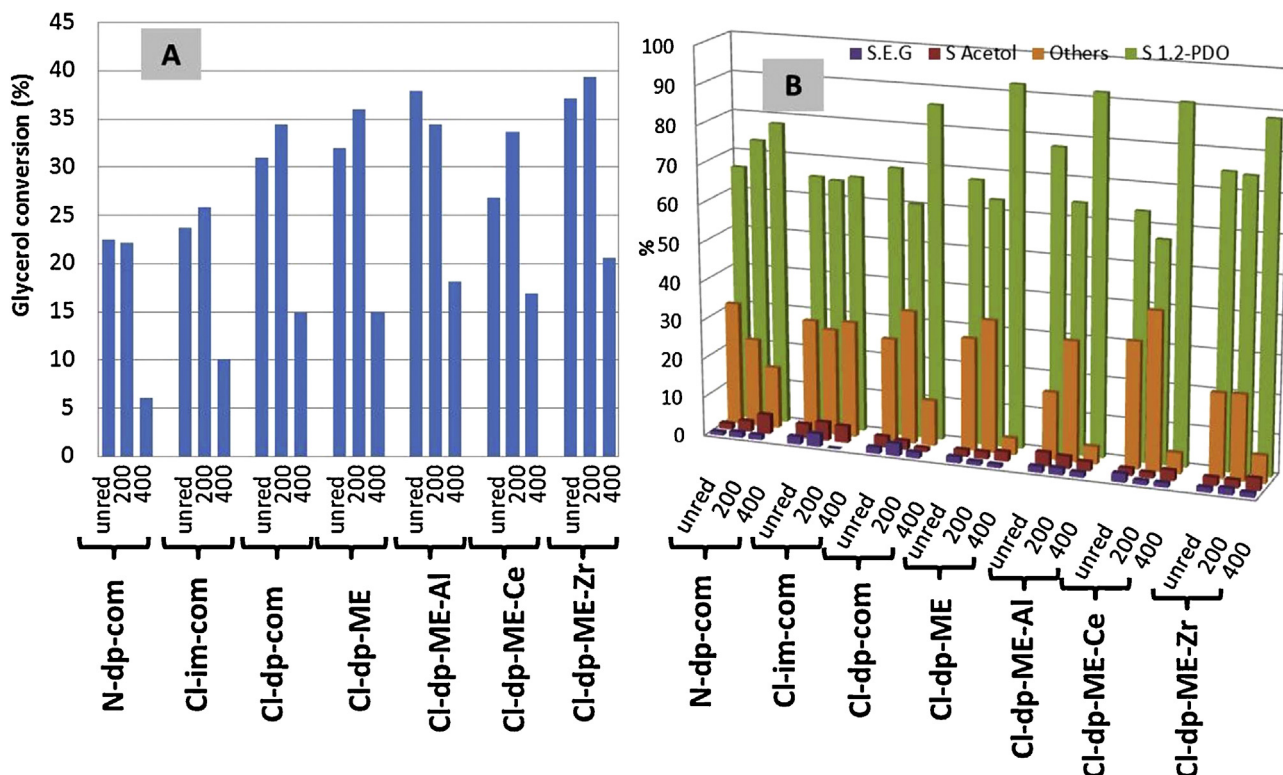


Fig. 11. Results for catalytic transformation of glycerol expressed in terms of conversion (A) and selectivity to ethylene glycol (EG), acetol, 1,2-PDO or others (B) for $t = 15$ h. Reaction conditions: 100 mg catalysts, 10 mL 1.36 M water solution of glycerol. 180°C and 6 bar of initial hydrogen pressure. Reaction time: 15 h.

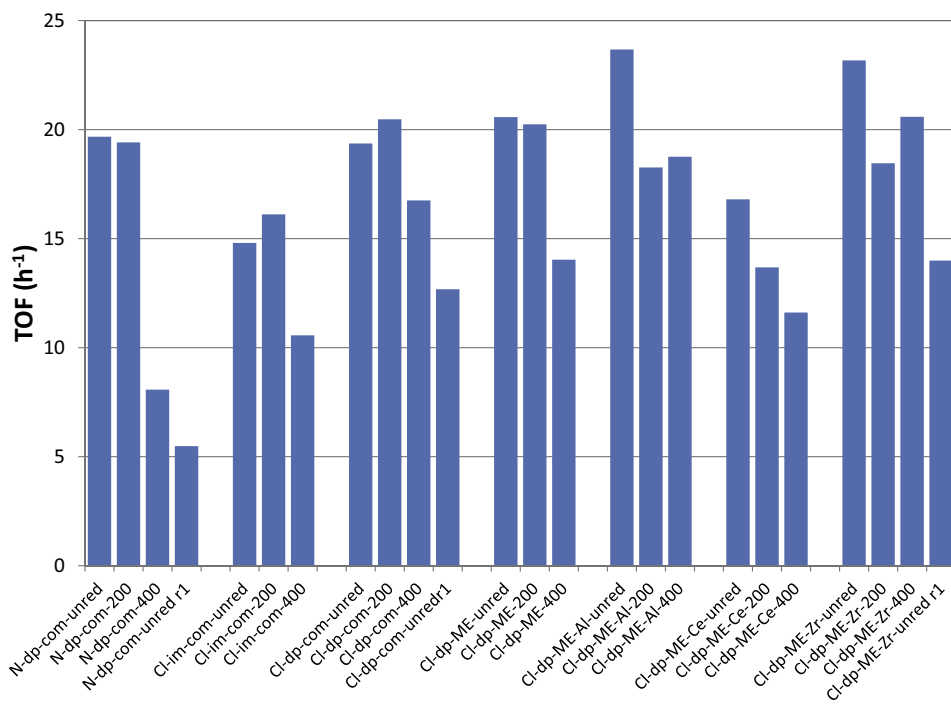


Fig. 12. Results obtained for catalytic transformation of glycerol expressed in terms of turnover frequencies (TOF) for $t = 15$ h. Reaction conditions: 100 mg catalysts, 10 mL 1.36 M water solution of glycerol, 180 °C and 6 bar of initial hydrogen pressure. Reaction time: 15 h. Data correspond to systems unreduced, reduced at 200 °C and 400 °C. In some cases results for the first reutilization of unreduced solids have been included (r1 suffix).

3.4. Mechanistic discussion

In order to cast further light on the process, some further studies were performed and a reaction mechanism suggested

(Scheme 1). Firstly, experiments at variable reaction times (1–15 h) were conducted starting from glycerol. The results showed that for Cl-containing solids, the selectivity to 1,2-PDO was particularly low during the first hours of reaction (see data for Cl-dp-com-unred in

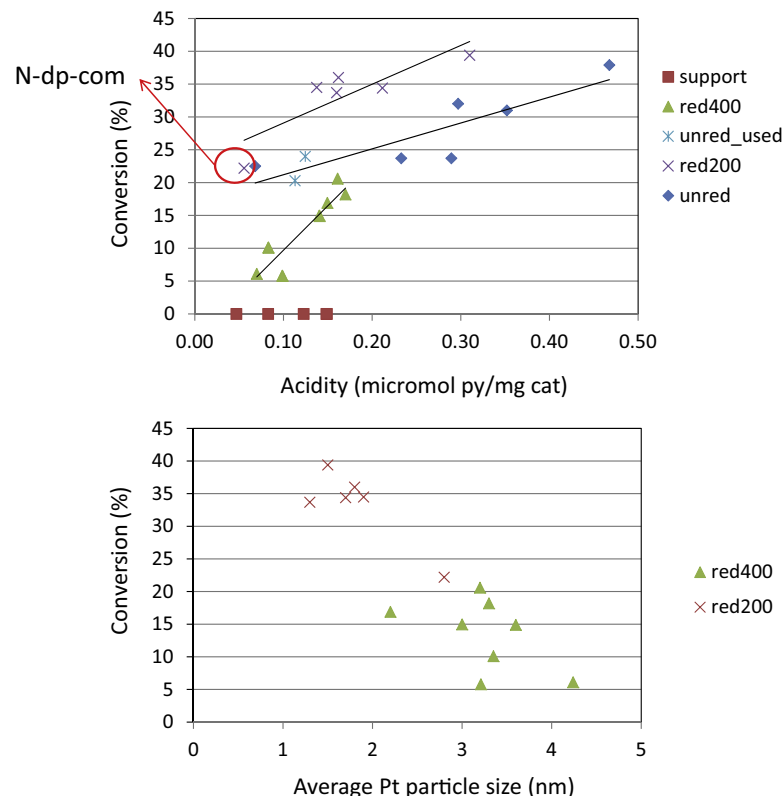


Fig. 13. Glycerol conversion as a function of acidity (micromoles of pyridine per mg of catalyst) or average particle size (in nm, as determined by TEM) for the different catalysts used in the present manuscript. Reaction conditions: 100 mg catalysts, 10 mL 1.36 M water solution of glycerol, 180 °C and 6 bar of initial hydrogen pressure. Reaction time: 15 h.

Table 3

Results obtained for glycerol transformation on Cl-dp-com and N-dp-com under standard conditions expressed as glycerol conversion % and selectivity to 1,2-PDO, acetol, ethylene glycol (EG) and other products. In some cases, results for characterization of the solids have been included.

Catalyst	GC-FID					% Pt	XPS			TPD pyridine	TEM
	Gly conv	Selectivity 1,2-PDO	Selectivity acetol	Selectivity EG	Selectivity others		Pt/Zn	Cl/Pt	Cl/Zn		
Cl-dp-com unred (fresh)	—	—	—	—	—	4.2	0.42	0.72	0.29	0.23	1.9
Cl-dp-com unred (1 h)	2.3	35.8	6.5	0.0	57.7	ND	0.28	0.11	0.03	0.11	ND
Cl-dp-com unred (5 h)	10.5	35.0	4.0	2.5	58.5	ND	ND	ND	ND	ND	ND
Cl-dp-com unred (10 h)	24.5	63.0	4.3	1.7	25.5	ND	ND	ND	ND	ND	ND
Cl-dp-com unred (15 h)	31.0	69.1	3.8	1.6	25.5	4.3	0.24	0.11	0.03	0.11	1.9
Cl-dp-com unred r1 (15 h)	20.3	71.9	2.7	0.6	24.5	ND	ND	ND	ND	ND	ND
Cl-dp-com unred r2 (15 h)	18.0	79.2	3.2	1.0	16.5	ND	ND	ND	ND	ND	ND
N-dp-com unred (fresh)	—	—	—	—	—	4.3	0.25	0	0	0.06	2.8
N-dp-com unred (5 h)	11.3	53.9	4.8	1.6	39.7	ND	ND	ND	ND	ND	ND
N-dp-com unred (15 h)	22.5	66.0	1.5	0.9	31.6	3.3	0.14	0	0	0.06	2.8
N-dp-com unred r1	8.8	80.7	5.3	0.3	13.7	ND	ND	ND	ND	ND	ND
N-dp-com unred r2	7.3	87.3	4.8	0.0	7.9	ND	ND	ND	ND	ND	ND

Table 3). This could be due to the presence of Cl ions on the surface favoring excessive hydrogenolysis and C–C cleavage [17,18]. Moreover, aqueous phase reforming (APR) is known to be favored on highly-dispersed catalysts as it is the case [16] (Scheme 1). Apparently, after 5 h of reaction the extent of C–C cleavage decreased thus resulting in an increase in selectivity to 1,2-PDO. Complementary XPS and TPD studies of pre-adsorbed pyridine (Table 3) showed that chlorine was almost lost from the catalyst surface within 1 h of reaction and that acidity had significantly decreased. These results suggest the possibility of acidic cracking occurring on strong acid sites which deactivate as reaction proceeds thus resulting in an increase in selectivity to 1,2-PDO. Interestingly, reutilization studies (Table 3) showed a drop in conversion which could be associated to the deactivation of those strong acid sites which could catalyze both C–C cleavage and dehydration of glycerol into acetol. The drop in conversion is accompanied by a significant increase in selectivity to 1,2-PDO. From Table 3 it is also evident that as reaction proceeds, there is a catalyst restructuring involving chlorine leaching and decoration of platinum particles by Zn (see decrease in Pt/Zn ratio), whereas Pt particle size remains constant. In the case of N-dp-com system, initial selectivity to 1,2-PDO is higher than that achieved on Cl-series, which again could be related to the absence of strong acid sites associated to chlorine as well as the higher Pt particle size which is detrimental to APR. Reuse of the systems led to a significant decrease in conversion which could be associated to the Pt leaching (compare %Pt as determined by ICP-MS of N-dp-com unred (fresh) and N-dp-com unred (15 h), Table 3), and decoration of Pt particles by Zn. The increase in selectivity with reuses could suggest some Pt–Zn strong metal–support interaction leading to active sites more selective to 1,2-PDO.

For similar conversion values, solids reduced at 400 °C exhibited a higher selectivity to 1,2-PDO than unred systems (Fig. 11 and Table 3). This suggests that changes occurring in the catalyst as reduction temperature is increased (Pt–Zn alloy formation, loss of acidity, increase in Pt particle size) leads to the prevalence or the formation of specific active sites for 1,2-PDO generation. Some other experiments were conducted starting from acetol. Production of 1,2-PDO from glycerol is known to occur through acetol, via dehydration of a primary hydroxyl group in glycerol. Moreover, dehydration of glycerol to acetol is slower than hydrogenation of acetol to 1,2-PDO [19]. In fact, if we start from 1.36 M acetol (the same concentration as for glycerol studies), conversion after 15 h is total, with selectivity to 1,2-PDO in the 83–86% range. The exception is Cl-im-com (91% conversion, 68% selectivity). Taking the example of Cl-dp-com-unred, selectivity at full conversion is

85.2%. When the reaction time is decreased to 3 h, the conversion and selectivity values on Cl-dp-com-unred are lower (74% and 85.5%, respectively). Reducing acetol initial concentration to 1/3 of its value, conversion after 3 h is 93% and selectivity 97%. In the case of acetol, GC-MS studies evidenced the formation of several C₄–C₉ liquid oxygenates, their relative percentage increasing with the reduction of hydrogen pressure or the increase in acetol initial concentration.

Finally, some reactions were carried out under nitrogen atmosphere. Activity order was coincident with that obtained under H₂ atmosphere (e.g. the most acidic solids, Cl-dp-com-Al-unred and Cl-dp-com-Zr-unred, were also the most active ones) though selectivity to 1,2-PDO decreased significantly because of APR and formation of C₄–C₉ liquid oxygenates.

4. Conclusions

Different ZnO solids (either alone or doped with Al, Zr or Ce) were synthesized through the microemulsion technique which allowed us to obtain similar particle sizes and textural properties. Platinum was subsequently incorporated from H₂PtCl₆ through deposition–precipitation or impregnation method. For comparative purposes, a system from Pt(NO₃)₄ was also obtained through deposition–precipitation method. Incorporation of platinum led to the creation of new (mainly Lewis) acid sites, particularly important in the case of chlorine-containing solids. Moreover, acidity is partly lost during reduction treatment or as the reaction proceeds which could be ascribed to both chlorine release and platinum decoration by the support (as evidenced by XPS). A direct relationship between acidity and glycerol conversion was found. Interestingly, supports were not active in the process which evidences the participation of the metal in the dehydration of glycerol to acetol. As regards selectivity to 1,2-PDO, it increases as reaction proceeds and acidity of solids decreases to the detriment of acidic cracking. This suggests that strong acid sites associated to chlorine are responsible for C–C cleavage and excessive hydrogenolysis, whereas dehydration of glycerol into acetol requires moderate acidity. Moreover, formation of Pt–Zn strong metal interaction is beneficial to 1,2-PDO selectivity.

Acknowledgements

The authors are thankful to Junta de Andalucía and FEDER funds (P08-FQM-3931 and P09-FQM-4781 projects) for financial support. SCAI at the University of Cordoba is also acknowledged for ICP-MS measurements and the use of TEM and XPS. Finally, the authors are

grateful to COST Action CM0903 for financial support, including a short-term scientific mission (STSM) of V. Montes.

References

- [1] Z. Yuan, P. Wu, J. Gao, X. Lu, Z. Hou, X. Xheng, *Catal. Lett.* 130 (2009) 261–265.
- [2] A. Marinas, P. Bruijnincx, J. Ftouni, F.J. Urbano, C. Pinel, *Catal. Today* 239 (2015) 31–37, <http://dx.doi.org/10.1016/j.cattod.2014.02.048>.
- [3] R. Rodrigues, N. Isoda, M. Gonçalves, F.C.A. Figueiredo, D. Mandelli, W.A. Carvalho, *Chem. Eng. J.* 198/199 (2012) 457–467.
- [4] M. Checa, F. Auneau, J. Hidalgo-Carrillo, A. Marinas, J.M. Marinas, C. Pinel, F.J. Urbano, *Catal. Today* 196 (2012) 101–100.
- [5] T. Miyazawa, Y. Kusunoki, K. Kunimori, K. Tomishige, *J. Catal.* 240 (2006) 213–221.
- [6] F. Auneau, C. Michel, F. Delbecq, C. Pinel, P. Sautet, *Chem. Eur. J.* 17 (2011) 14288–14299.
- [7] J. Chaminand, L. Djakovitch, P. Gallezot, P. Marion, C. Pinel, C. Rosier, *Green Chem.* 6 (2004) 359–361.
- [8] F. Auneau, S. Noël, G. Aubert, M. Besson, L. Djakovitch, C. Pinel, *Catal. Commun.* 16 (2011) 144–149.
- [9] F. Vila, M. López Granados, M. Ojeda, J.L.G. Fierro, R. Mariscal, *Catal. Today* 187 (2012) 122–128.
- [10] Z. Huang, F. Cui, J. Xue, J. Zuo, J. Chen, C. Xia, *Catal. Today* 183 (2012) 42–51.
- [11] I. Gandarias, P.L. Arias, J. Requies, M. El Doukkali, M.B. Güemez, *J. Catal.* 282 (2011) 237–247.
- [12] L. Ma, D. He, *Catal. Today* 149 (2010) 148–156.
- [13] A. Iriondo, J.F. Cambra, V.L. Barrio, M.B. Guemez, P.L. Arias, M.C. Sanchez-Sánchez, R.M. Navarro, J.L.G. Fierro, *Appl. Catal. B: Environ.* 106 (2011) 83–93.
- [14] J. Ten Dam, F. Kapteijn, K. Djanashvili, U. Hanefeld, *Catal. Commun.* 13 (2011) 1–5.
- [15] A. Wawrzetz, B. Peng, A. Hrabar, A. Jentys, A.A. Lemonidou, J.A. Lercher, *J. Catal.* 269 (2010) 411–420.
- [16] M.L. Barbelli, F. Pompeo, G.F. Santori, N.N. Nichio, *Catal. Today* 213 (2013) 58–64.
- [17] S.N. Delgado, D. Yap, L. Vivier, C. Especel, *J. Mol. Catal. A: Chem.* 367 (2013) 89–98.
- [18] E.S. Vasiliadou, E. Heracleous, I.A. Vasalos, A.A. Lemonidou, *Appl. Catal. B: Environ.* 92 (2009) 90–99.
- [19] J. ten Dam, U. Hanefeld, *ChemSusChem* 4 (2011) 1017–1034.
- [20] S. Zhu, Y. Qiu, Y. Zhu, S. Hao, H. Zheng, Y. Li, *Catal. Today* 212 (2013) 120–126.
- [21] B. Peng, C. Zhao, I. Mejía-Centeno, G.A. Fuentes, A. Jentys, J.A. Lercher, *Catal. Today* 183 (2012) 3–9.
- [22] Y. Feng, H. Yin, A. Wang, L. Shen, L. Yu, T. Jiang, *Chem. Eng. J.* 168 (2011) 403–412.
- [23] I. Gandarias, P.L. Arias, J. Requies, M.B. Güemez, J.L.G. Fierro, *Appl. Catal. B: Environ.* 87 (2010) 248–256.
- [24] V. Montes, M. Checa, A. Marinas, M. Boutonnet, J.M. Marinas, F.J. Urbano, S. Járas, C. Pinel, *Catal. Today* 223 (2014) 129–137.
- [25] M. Sanchez-Dominguez, K. Pemartin, M. Boutonnet, *Curr. Opin. Colloid Interface Sci.* 17 (2012) 297–305.
- [26] M. Sanchez-Dominguez, L.F. Liotta, G. Di Carlo, G. Pantaleo, A.M. Venezia, C. Solans, M. Boutonnet, *Catal. Today* 158 (2010) 35–43.
- [27] A.S. Shaporev, V.K. Ivanov, A.E. Baranchikov, O.S. Polezhaeva, Y.D. Tret'yakov, *Russian J. Inorg. Chem.* 52 (2007) 1811–1816.
- [28] G. Patrinoiu, J.M. Calderón-Moreno, D.C. Culita, R. Birjega, R. Ene, O. Carp, *Solid State Sci.* 23 (2013) 58–64.
- [29] F. Xiao, B. Zhang, C. Lee, *J. Environ. Sci.* 20 (2008) 907–914.
- [30] M.A. Aramendia, V. Boráu, C. Jiménez, A. Marinas, J.M. Marinas, J.A. Navío, J.R. Ruiz, F.J. Urbano, *Colloids Surf. A: Physicochem. Eng. Aspects* 234 (2004) 17–25.
- [31] D. Raoufi, T. Raoufi, *Appl. Surf. Sci.* 255 (2009) 5812–5817.
- [32] Y. Wei, Z. Zhao, T. Li, J. Liu, A. Duan, G. Jiang, *Appl. Catal. B: Environ.* 146 (2014) 57–70.
- [33] J. Hidalgo-Carrillo, A. Marinas, J.M. Marinas, J.J. Delgado, R. Raya-Miranda, F.J. Urbano, *Appl. Catal. B: Environ.* 154–155 (2014) 369–378.
- [34] M. Abid, V. Paul-Boncour, R. Touroude, *Appl. Catal. A: Gen.* 297 (2006) 48–59.
- [35] S. Subramanian, Platin. *Metals Rev.* 36 (1992) 98–103.
- [36] J. Silvestre-Albero, F. Coloma, A. Sepúlveda-Escribano, F. Rodríguez-Reinoso, *Appl. Catal. A: Gen.* 304 (2006) 159–167.
- [37] P.S. Querino, J.R.C. Bispo, M. do Carmo Rangel, *Catal. Today* 107–108 (2005) 920–925.
- [38] J. Hidalgo-Carrillo, M.A. Aramendia, A. Marinas, J.M. Marinas, F.J. Urbano, *Appl. Catal. A: Gen.* 385 (2010) 190–200.
- [39] G.E. McGuire, G.K. Schweitzer, Thomas A. Carlson, *Inorg. Chem.* 12 (1973) 2450–2453.
- [40] A. Salaün, M. Veillerot, F. Pierre, E. Souchier, V. Jousseaume, *ECS J. Solid State Sci. Technol.* 3 (2014) N39–N45.
- [41] G. Berhault, M. Lacroix, M. Breysse, F. Maugé, J.-C. Lavalle, H. Nie, L. Qu, *J. Catal.* 178 (1998) 555–565.
- [42] B. Li, R.D. Gonzalez, *Catal. Today* 46 (1998) 55–67.